ACS Macro Letters

pubs.acs.org/macroletters Letter

Critical-Like Gelation Dynamics in Cellulose Nanocrystal Suspensions

Lise Morlet-Decarnin, Thibaut Divoux, and Sébastien Manneville*

Cite This: ACS Macro Lett. 2023, 12, 1733−1738 Read Online

ACCESS | Metrics & More | Article Recommendations | Supporting Information

ABSTRACT: We use time-resolved mechanical spectroscopy to offer a detailed picture of the gelation dynamics of cellulose nanocrystal (CNC) suspensions following shear cessation in the presence of salt. CNCs are charged, rodlike colloids that self-assemble into various phases, including physical gels serving as soft precursors for biosourced composites. Here, a series of linear viscoelastic spectra acquired across the sol−gel transition of CNC suspensions are rescaled onto two master curves that correspond to a viscoelastic liquid state prior to gelation and to a soft solid state after gelation. These two states are separated by a critical gel point, where all rescaling parameters diverge in an asymmetric fashion yet with exponents that obey hyperscaling relations consistent with previous works on isotropic colloids and polymer gels. Upon varying the salt content, we further show that these critical-like dynamics result in both time−connectivity and time−concentration superposition principles.

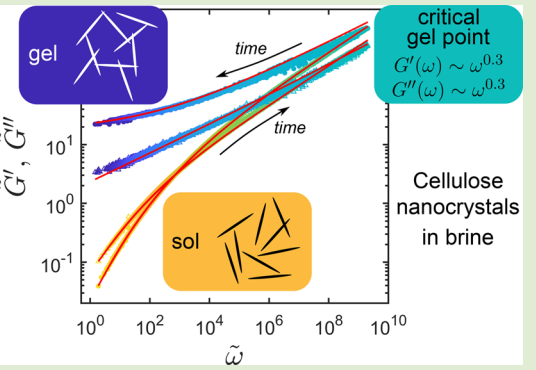

Colloidal nanocrystals are rodlike crystalline clusters of atoms with sizes ranging from tens to a few hundred nanometers.[1] These colloids with tunable surface chemistry can be either synthesized or extracted from natural products, such as biopolymers. When dispersed into a suspending fluid, colloidal nanocrystals can self-assemble into micro- or meso-structures with outstanding optical and mechanical properties relevant for applications in optics, electronics, sensing, and biomedicine.[2,3] Several applications, such as catalysis and optoelectronics, rely on the formation of physical gels, i.e., space-spanning networks of colloidal nanocrystals, which behave mechanically as soft solids. While much is known about the different ways and means to induce gelation in colloidal nanocrystals,[4−6] very few studies have characterized their gelation dynamics and the emergence of solid-like properties upon their self-assembly. Yet, understanding such dynamics is crucial for tailoring the microstructure of nanocrystal gels serving as soft precursors for harder materials.

Here, we perform a time-resolved mechanical spectroscopy study of the sol−gel transition in cellulose nanocrystals (CNCs). CNCs are biosourced, biodegradable, and biocompatible nanocrystals, which consist of rigid, negatively charged rodlike particles of typical length 100−500 nm and diameter 5−20 nm.[1,7−13] Aqueous dispersions of CNCs display a rich phase diagram including liquid crystalline phases, gels, and glasses.[14,15] In practice, in dilute CNC suspensions, gelation is induced by adding salt, hence screening the electrostatic repulsion between the CNCs that aggregate via hydrogen bonds and van der Waals interactions.[16−18] In this paper, using time-resolved mechanical spectroscopy, we aim to provide a detailed dynamical picture of the sol−gel transition of CNC dispersions following flow cessation in the presence of salt. Following previous works on *time−connectivity* superposition, also referred to as time−cure superposition,[19−22] viscoelastic spectra acquired across the sol−gel transition are rescaled onto two remarkable master curves that extend on each side of a critical gel point. These master curves are compactly described by two fractional mechanical models, which correspond respectively to a viscoelastic liquid state and to a soft solid state and which share a common element capturing the power−law rheology of the CNC dispersion at the gel point. Moreover, varying the salt content within the CNC dispersion reveals that the pregel viscoelastic liquid and the postgel viscoelastic solid can also be rescaled onto two universal master curves, following a *time−concentration* superposition principle. Finally, we discuss the exponents that characterize the present critical-like gelation dynamics in view of the literature on other chemical and physical gels.

CNC gels are prepared using a commercial 6.4 wt % aqueous suspension of CNCs extracted from wood (CelluForce). The suspension is diluted with salt water to obtain samples containing 2 wt % of CNCs and salt (NaCl, Merck) in

Received: September 8, 2023
Revised: November 30, 2023
Accepted: December 1, 2023

https://doi.org/10.1021/acsmacrolett.3c00536
ACS Macro Lett. 2023, 12, 1733−1738

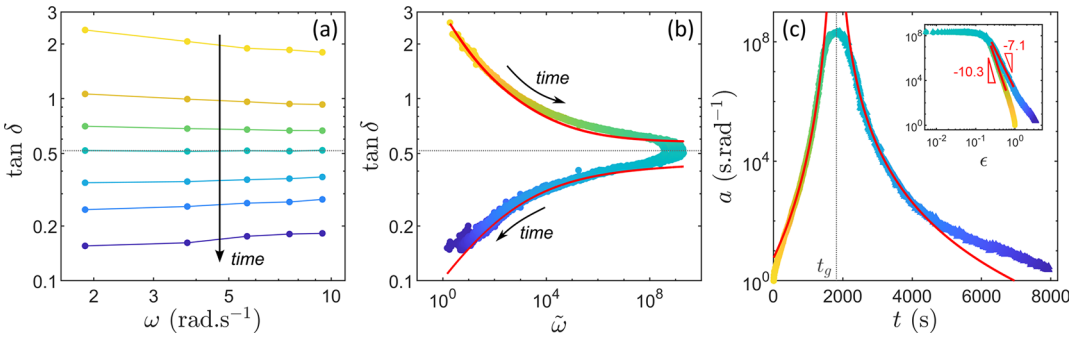

Figure 1. Time-resolved mechanical spectroscopy of the sol−gel transition in a CNC suspension. (a) Dependence of the loss factor tan δ on the frequency ω at different points in time (t = 10 to 8000 s, from yellow to dark blue) across the sol−gel transition of a 2 wt % CNC suspension containing 15 mM of NaCl. The gel point is highlighted by the horizontal dashed line. (b) Master curve for the loss factor tan δ vs reduced frequency $\tilde{\omega} = a(t)\omega$. The red curves show the best fits of the data respectively by a fractional Maxwell model for $t < t_g$ (upper curve) and by a fractional Kelvin−Voigt model for $t > t_g$ (lower curve). (c) Time dependence of the shift factor a. The initial value is arbitrarily taken as $a(0) = 1$ s·rad^{-1}. The vertical dashed line highlights the gelation time t_g = 1820 s. Inset: a vs $\varepsilon = |t - t_g|/t_g$ in logarithmic scales. The red curves in both the main graph and the inset show the best power−law fits of the data, $a \sim \varepsilon^{-y}$, with exponents y_l = 10.3 for $t < t_g$ and y_g = 7.1 for $t > t_g$.

amounts ranging from 12 to 22 mM. The sample is homogenized under high shear using mechanical stirring at 2070 rpm (IKA RW 20 Digital mixer equipped with an R1402 blade dissolver) before, during, and after salt addition for about 5 min at each step. Finally, the sample is stored in the refrigerator for 24 h before being used. At a concentration of 2 wt %, CNCs are expected to overlap, and in the above range of salt concentrations, CNCs form colloidal gels (see also Supporting Information for more experimental details).[14−16] The mechanical properties of the present CNC suspensions are probed during gelation using a stress-controlled rheometer (AR-G2, TA Instruments) equipped with a smooth cylindrical Taylor-Couette geometry (height of 58 mm, inner rotating cylinder of radius 24 mm, outer fixed cylinder of radius 25 mm, and gap e = 1 mm). The cell is closed by a homemade lid, and the temperature is controlled to T = 23 ± 0.1 °C, thanks to a water circulation around the cell. This setup allowed us to study the same sample over several hours without any artifact due to evaporation.

After being loaded in the shear cell, each sample is first fully fluidized under a high shear rate $\dot{\gamma}$ = 1000 s^{-1} during 60 s, before being quenched by setting $\dot{\gamma} = 0$, which defines the time origin t = 0 s. Upon the cessation of shear, the initially liquid CNC suspension slowly reassembles into a physical gel. This sol−gel transition is monitored over up to 5 × 10^4 s thanks to time-resolved mechanical spectroscopy.[23] In practice, cycles of small-amplitude oscillatory stress measurements are performed over five discrete frequencies ω ranging between 0.3 and 1.5 Hz. This yields one viscoelastic spectrum, defined by the elastic modulus G' and the viscous modulus G'' as a function of ω, at every δt_{exp} = 5 s. These frequencies are purposely chosen such that the sample properties do not evolve significantly over this time scale, i.e., $(\delta t_{exp}/G')\ (\partial G'/\partial t) \ll 1$.[23,24]

Figure 1 illustrates the gelation dynamics of a 2 wt % CNC suspension containing 15 mM of salt. The frequency dependence of the loss factor tan $\delta = G''/G'$ is reported in Figure 1(a) at various points in time across the sol−gel transition. This first allows us to identify the "true" gel point[25] defined as the time t_g = 1820 s when tan δ is frequency independent [see gray dashed line at tan δ = 0.52 in Figure 1(a)]. Second, tan $\delta(\omega)$ shows two opposite trends on each side of the gel point: it decreases with ω for $t < t_g$, while it increases with ω for $t > t_g$. We also note that the slope of tan δ vs ω continuously goes from negative to positive across the gel point. This prompts us to apply a time-dependent multiplicative factor $a(t)$ to the frequency ω, in order to collapse the tan δ data measured at different points in time onto a single curve,[26] thus revealing the systematic dynamics of the gelation process. As shown in Figure 1(b), this rescaling leads to two master curves, one on each side of the gel point, composed of more than 1600 spectra spanning 9 orders of magnitude in rescaled dimensionless frequency $\tilde{\omega} = a(t)\omega$, and describing the entire gelation process. This result points to a time−connectivity superposition principle, as previously identified in polymer gels and colloidal gels made of spherical, rodlike, or fiber-like particles,[22,27−32] and highlights the self-similar evolution of the sample viscoelastic properties on each side of the gel point. Quite remarkably, the time-dependent shift factor $a(t)$ displays a power−law divergence in the vicinity of the gel point, with a critical exponent y_l = 10.3 for $t < t_g$ and y_g = 7.1 for $t > t_g$ [see Figure 1(c)].

As shown in Figure 2, we further construct a master curve for both viscoelastic moduli G' and G'' vs $\tilde{\omega}$ by shifting each instantaneous viscoelastic spectrum vertically thanks to a multiplicative coefficient $b(t)$. These master curves span over 5 orders of magnitude in rescaled moduli $\tilde{G}' = b(t)G'$ and $\tilde{G}'' = b(t)G''$, which confirms that time−connectivity superposition applies. Here again, the shift factor $b(t)$ follows critical-like dynamics around t_g, yet with exponents z_l = 3.0 for $t < t_g$ and z_g = 1.9 for $t > t_g$ that are about three times smaller than those found for $a(t)$ [see inset in Figure 2]. Moreover, the 9 orders of magnitude covered in rescaled frequencies indicate a very wide range of distinct relaxation processes in the sample microstructure. Such a broad relaxation spectrum is often compactly described by fractional models,[31,33,34] which introduce "spring-pots" as key rheological elements. A spring-pot is defined by a constitutive equation that relates the stress σ and the strain γ through a fractional derivative,[33] $\sigma = \mathbb{G} d^{\beta}\gamma/dt^{\beta}$, where $\mathbb{G}$ is a "quasi-property" with dimension Pa·s$^{\beta}$, and $\beta \in [0, 1]$ is the order of the derivative. In the limit $\beta \to 0$ (respectively $\beta \to 1$), the spring-pot corresponds to a purely elastic (respectively viscous) response. For $0 < \beta < 1$, it displays a power−law viscoelastic spectrum $G' \sim G'' \sim \omega^{\beta}$, or equivalently a power−law relaxation modulus $G(t) \sim t^{-\beta}$, and a frequency-independent phase angle $\delta = \beta\pi/2$. Such power−law rheology is common to all "critical gels" that form self-similar

https://doi.org/10.1021/acsmacrolett.3c00536
ACS Macro Lett. 2023, 12, 1733−1738

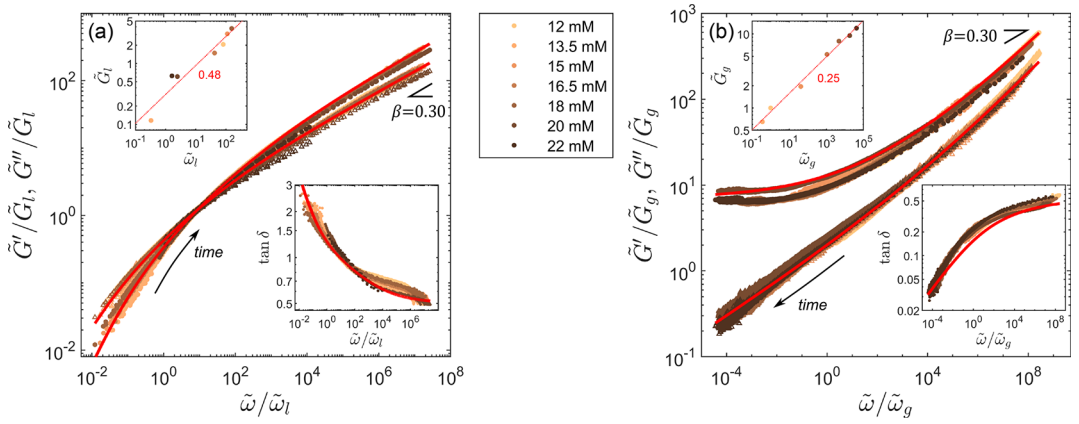

Figure 2. Master curves obtained by rescaling the elastic modulus G' (•) and the viscous modulus G'' (△) by the same multiplicative factor $b(t)$, i.e., $\tilde{G}' = b(t)G'$ and $\tilde{G}'' = b(t)G''$. The horizontal axis is the rescaled frequency $\tilde{\omega} = a(t)\omega$ as defined in Figure 1. The red lines show the best fits of the data by a fractional Maxwell model for $t < t_g$ and by a fractional Kelvin−Voigt model for $t > t_g$ (see sketches of the mechanical models as insets). Inset: time dependence of the shift factor b. The initial value is arbitrarily taken as $b(0) = 1$ Pa^{-1}. The red curves show the best power−law fits of the data, $b \sim \varepsilon^{-z}$, where $\varepsilon = |t - t_g|/t_g$, with exponents $z_l = 3.0$ for $t < t_g$ and $z_g = 1.9$ for $t > t_g$. The vertical dashed line highlights the gelation time t_g = 1820 s. Same experiment as in Figure 1.

percolated networks at the gel point[19,35] and for which the exponent β is referred to as the critical relaxation exponent.[36,37] Therefore, the fractional approach is ideally suited to characterize the mechanical response of colloidal gels, from their critical gel point and beyond.[31,38,39]

Here, we fit the master curves on each side of the gel point by two five-parameter fractional models, respectively: a fractional Maxwell model for $t < t_g$, which captures the liquid-like viscoelasticity of the CNC suspension prior to the gel point, and a fractional Kelvin−Voigt model for $t > t_g$, which captures the solid-like viscoelastic behavior past the gel point (see, respectively, lower and upper sketches in Figure 2). The reader is referred to the Supporting Information for full mathematical details on the models. A crucial result is that both models share a common spring-pot element $(\mathbb{G},\beta)$, which is alone responsible for capturing the gel point, here with a critical relaxation exponent $\beta = 0.30$ that corresponds to a value of $\tan(\beta\pi/2) = 0.51$, which is fully consistent with the value of $\tan\delta$ observed at the gel point in Figure 1(a). The fits by the two models are shown with red lines in Figure 2 for the rescaled viscoelastic moduli and in Figure 1(b) for the corresponding loss factor. The agreement between theory and experiment is excellent, which provides strong support for interpreting the gelation dynamics in terms of two consecutive fractional mechanical behaviors separated by a critical gel point.

In order to explore the impact of the salt content on the master curves reported in Figure 2, the above analysis was repeated for CNC dispersions with salt concentrations ranging between 12 and 22 mM. In all cases, we can unambiguously identify a critical gel point associated with a gelation time t_g. Upon increasing the salt concentration, the gelation dramatically accelerates due to the stronger screening of electrostatic interactions [see Supporting Figure S1(a)], as already reported not only in CNC suspensions[17,40] but also for other types of colloids.[41,42] Yet, for all salt contents, a master curve similar to that of Figure 2 can be built, for which the above fractional approach provides very good fits (see Supporting Figure S2). Strikingly, at the gel point, the power−law dependence of the viscoelastic moduli with frequency is independent of the salt content, with an exponent $\beta = 0.30 \pm 0.03$ [see Supporting Figure S1(b)]. This demonstrates the robustness of both the time−connectivity superposition principle and the microstructure of the percolated network formed at the gel point to a change in the strength of electrostatic interactions between the CNCs. Indeed, the exponent β can be related to the fractal dimension d_f of the stress-bearing network at the gel point.[31,43] Using the relation proposed in ref 43 for screened interactions, we obtain $d_f = 2.2$ for $\beta = 0.30$, which is compatible with independent neutron and light scattering measurements that yield $1.6 \lesssim d_f \lesssim 2.1$.[16]

Furthermore, we note that beside β, the fractional derivative orders α and ξ of the two other spring-pots involved in our fractional models, which respectively control the low-frequency viscoelastic behavior of the viscoelastic liquid for $t < t_g$ and of the soft solid for $t > t_g$, do not significantly depend on the salt content either (see Supporting Table S2). This suggests again rescaling all master curves, first by collapsing all loss factors $\tan\delta(\tilde{\omega})$ thanks to a simple rescaling of $\tilde{\omega}$ into $\tilde{\omega}/\tilde{\omega}_i$ (see lower insets in Figure 3), and then by normalizing both rescaled viscoelastic moduli $\tilde{G}'$ and $\tilde{G}''$ with a factor $\tilde{G}_i$, where $i = l$ ($i = g$ respectively) for the liquid (gel respectively) state. As shown in Figure 3, the result is two remarkable universal master curves for the dynamics both before and after the gel point, spanning over 12 orders of magnitude in rescaled frequency and four decades in viscoelastic moduli. These master curves are consistently nicely fitted by a fractional Maxwell model for $t < t_g$ and by a fractional Kelvin−Voigt model for $t > t_g$, with $\beta = 0.30$, $\alpha = 0.64$, and $\xi = 0.19$. The shift factors $\tilde{G}_i'$ and $\tilde{\omega}_i$ appear to be linked by two different, nontrivial power laws with exponents of roughly 1/2 in the pregel state and 1/4 in the postgel state (see upper insets in Figure 3).

Finally, the superposition principles revealed in the present experiments are derived from the critical-like dynamics of the gelation process around the gel point that are characterized by four critical exponents, which values are independent of the salt content [see Supporting Figure S1(c)]: $y_l = 9.4 \pm 0.5$, $y_g = 7.4 \pm 0.5$, $z_l = 2.8 \pm 0.2$, and $z_g = 2.1 \pm 0.2$ when averaged over all concentrations in NaCl. These exponents are linked to those introduced classically in the literature on chemical and

https://doi.org/10.1021/acsmacrolett.3c00536
ACS Macro Lett. 2023, 12, 1733−1738

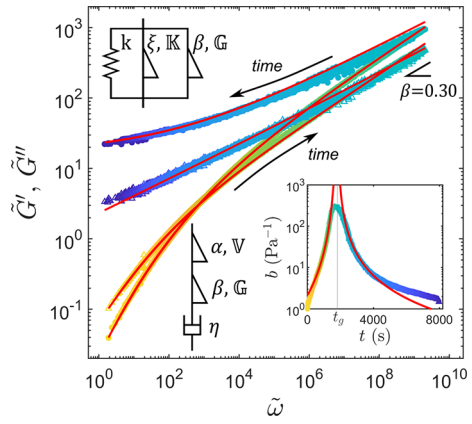

Figure 3. Rescaled master curves for the viscoelastic spectra measured (a) before and (b) after the gel point on CNC suspensions for salt concentrations ranging between 12 mM and 22 mM. Lower insets: $\tan\delta = \tilde{G}''/\tilde{G}' = G''/G'$ vs $\tilde{\omega}/\tilde{\omega}_i$. Upper insets: shift factors $\tilde{G}_i$ vs $\tilde{\omega}_i$ for the various salt concentrations, together with their best power–law fits (red dotted lines). The indices $i = l$ and $i = g$ respectively denote the pregel liquid state in (a) and the postgel solid state in (b). The red curves show the best fits of the data with a fractional Maxwell model for $t < t_g$ in (a) and with a fractional Kelvin–Voigt model for $t > t_g$ in (b). The data for a salt content of 12 mM were chosen as a reference to construct the master curves. Color code for the concentration as indicated in the legend. Elastic and viscous moduli are shown with • and △, respectively.

physical gels based on percolation theory.[22,25,27,36,37,44−49] In particular, the exponents y_l and y_g associated with the frequency shift factor $a(t)$ in Figure 1 correspond to the divergence of the longest relaxation time in the system, respectively, before and after the gel point. Here, while most previous works have postulated a symmetric divergence, i.e., $y_l = y_g$, we find that the pregel exponent is systematically larger than its postgel counterpart by about 20%, out of the range of experimental uncertainty. A similar difference is found between the exponents z_l and z_g derived in Figure 2 from shift factor $b(t)$ for viscoelastic moduli. Whether such asymmetry in the critical behavior close to gelation is specific to CNCs or general to rodlike colloids is an open issue. Moreover, z_l and z_g relate to the exponents associated with the pregel divergence of the zero-shear viscosity, $\eta_0 \sim \varepsilon^{-s}$, and with the postgel growth of the zero-frequency elastic modulus, $G_e \sim \varepsilon^z$, through $z_g = z$ and $z_l = y_l - s$. Based on similarity arguments, the exponents s and z were shown to be linked to the rheological exponent β at the gel point through two hyperscaling relations,[36,46] $y_l = s/(1-\beta)$ and $y_g = z/\beta$, which simply rewrite to $\beta = z_l/y_l = z_g/y_g$ in the present notations. Using the above average values of the various exponents, we get $z_l/y_l \simeq 0.29$ and $z_g/y_g \simeq 0.28$, very close to $\beta \simeq 0.30$ and thus consistent with the predicted hyperscaling and with previous experimental results for microrheology on colloidal rods.[50]

To conclude, our results demonstrate that the gelation of CNC suspensions after shear cessation involves critical-like dynamics, where the salt content drives only the aggregation kinetics. While similar criticality has already been reported many times in chemical and physical gels, our experiments address the case of rod-like colloids for the first time thanks to a systematic rescaling approach, which does not require estimation of a zero-shear viscosity and a zero-frequency modulus by extrapolating viscoelastic spectra at low frequencies. The present study also highlights several peculiarities, including asymmetry in the pregel and postgel exponents and a surprisingly robust time–concentration superposition principle, which call for a microscopic description of the evolution of the colloidal nanorod network across the sol–gel transition, e.g., through time-resolved small-angle scattering. Such complementary microstructural information will help identify a possible universality class for gels made of colloidal nanorods based on the critical exponents and on the fractal features of the space-spanning network.

■ ASSOCIATED CONTENT

Supporting Information

The Supporting Information is available free of charge at https://pubs.acs.org/doi/10.1021/acsmacrolett.3c00536.

Supporting text, figures, and tables providing additional details on the materials and methods, on fractional mechanical models, on the data analysis, and on the fitting procedures (PDF)

■ AUTHOR INFORMATION

Corresponding Author

Sébastien Manneville − *ENSL, CNRS, Laboratoire de Physique, F-69342 Lyon, France; Institut Universitaire de France (IUF),* https://www.iufrance.fr/; orcid.org/0000-0002-4706-885X; Email: sebastien.manneville@ens-lyon.fr

Authors

Lise Morlet-Decarnin − *ENSL, CNRS, Laboratoire de Physique, F-69342 Lyon, France*

Thibaut Divoux − *ENSL, CNRS, Laboratoire de Physique, F-69342 Lyon, France;* orcid.org/0000-0002-6777-5084

Complete contact information is available at: https://pubs.acs.org/10.1021/acsmacrolett.3c00536

Author Contributions

CRediT: **Lise Morlet-Decarnin** data curation, formal analysis, investigation, methodology, software, visualization, writing-original draft; **Thibaut Divoux** conceptualization, formal analysis, investigation, methodology, supervision, validation, writing-original draft; **Sebastien Manneville** conceptualization, formal analysis, funding acquisition, methodology, project administration, resources, supervision, validation, writing-review & editing.

Notes

The authors declare no competing financial interest.

■ ACKNOWLEDGMENTS

The authors thank I. Capron, B. Jean, and F. Pignon for fruitful discussions. This work was funded by the Institut Universitaire de France (IUF). L. M.-D. also acknowledges financial support from École Normale Supérieure de Lyon.

■ REFERENCES

(1) Trache, D.; Tarchoun, A. F.; Derradji, M.; Hamidon, T. S.; Masruchin, N.; Brosse, N.; Hussin, M. H. Nanocellulose: From Fundamentals to Advanced Applications. *Front. Chem.* **2020**, *8*, 392.

(2) Parak, W. J.; Gerion, D.; Pellegrino, T.; Zanchet, D.; Micheel, C.; Williams, S. C.; Boudreau, R.; Gros, M. A. L.; Larabell, C. A.; Alivisatos, A. P. Biological applications of colloidal nanocrystals. *Nanotechnology* **2003**, *14*, R15–R27.

(3) Boles, M. A.; Engel, M.; Talapin, D. V. Self-Assembly of Colloidal Nanocrystals: From Intricate Structures to Functional Materials. *Chem. Rev.* **2016**, *116*, 11220−11289.
(4) Sayevich, V.; Cai, B.; Benad, A.; Haubold, D.; Sonntag, L.; Gaponik, N.; Lesnyak, V.; Eychmüller, A. 3D Assembly of All-Inorganic Colloidal Nanocrystals into Gels and Aerogels. *Angew. Chem., Int. Ed.* **2016**, *55*, 6334−6338.
(5) Green, A. M.; Ofosu, C. K.; Kang, J.; Anslyn, E. V.; Truskett, T. M.; Milliron, D. J. Assembling Inorganic Nanocrystal Gels. *Nano Lett.* **2022**, *22*, 1457−1466.
(6) Berestok, T.; Guardia, P.; Ibáñez, M.; Meyns, M.; Colombo, M.; Kovalenko, M. V.; Peiró, F.; Cabot, A. Electrostatic-Driven Gelation of Colloidal Nanocrystals. *Langmuir* **2018**, *34*, 9167−9174.
(7) Habibi, Y.; Lucia, L. A.; Rojas, O. J. Cellulose nanocrystals: chemistry, self-assembly, and applications. *Chem. Rev.* **2010**, *110*, 3479−3500.
(8) Lahiji, R. R.; Xu, X.; Reifenberger, R.; Raman, A.; Rudie, A.; Moon, R. J. Atomic Force Microscopy Characterization of Cellulose Nanocrystals. *Langmuir* **2010**, *26*, 4480−4488.
(9) Dufresne, A. Nanocellulose: a new ageless bionanomaterial. *Mater. Today* **2013**, *16*, 220−227.
(10) Lagerwall, J. P. F.; Schütz, C.; Salajkova, M.; Noh, J.; Hyun Park, J.; Scalia, G.; Bergström, L. Cellulose nanocrystal-based materials: from liquid crystal self-assembly and glass formation to multifunctional thin films. *NPG Asia Mater.* **2014**, *6*, No. e80.
(11) Klemm, D.; Cranston, E. D.; Fischer, D.; Gama, M.; Kedzior, S. A.; Kralisch, D.; Kramer, F.; Kondo, T.; Lindström, T.; Nietzsche, S.; Petzold-Welcke, K.; Rauchfuß, F. Nanocellulose as a natural source for groundbreaking applications in materials science: Today's state. *Mater. Today* **2018**, *21*, 720−748.
(12) Li, M.; Wu, Q.; Moon, R. J.; Hubbe, M. A.; Bortner, M. J. Rheological Aspects of Cellulose Nanomaterials: Governing Factors and Emerging Applications. *Adv. Mater.* **2021**, *33*, 2006052.
(13) Yucel, S.; Moon, R. J.; Johnston, L. J.; Yucel, B.; Kalidindi, S. R. Semi-automatic image analysis of particle morphology of cellulose nanocrystals. *Cellulose* **2021**, *28*, 2183−2201.
(14) Xu, Y.; Atrens, A. D.; Stokes, J. R. "Liquid, gel and soft glass" phase transitions and rheology of nanocrystalline cellulose suspensions as a function of concentration and salinity. *Soft Matter* **2018**, *14*, 1953−1963.
(15) Xu, Y.; Atrens, A. D.; Stokes, J. R. A review of nanocrystalline cellulose suspensions: Rheology, liquid crystal ordering and colloidal phase behaviour. *Adv. Colloid Interface Sci.* **2020**, *275*, 102076.
(16) Cherhal, F.; Cousin, F.; Capron, I. Influence of charge density and ionic strength on the aggregation process of cellulose nanocrystals in aqueous suspension, as revealed by small-angle neutron scattering. *Langmuir* **2015**, *31*, 5596−5602.
(17) Peddireddy, K. R.; Capron, I.; Nicolai, T.; Benyahia, L. Gelation kinetics and network structure of cellulose nanocrystals in aqueous solution. *Biomacromolecules* **2016**, *17*, 3298−3304.
(18) Abbasi Moud, A.; Kamkar, M.; Sanati-Nezhad, A.; Hejazi, S. H.; Sundararaj, U. Nonlinear viscoelastic characterization of charged cellulose nanocrystal network structure in the presence of salt in aqueous media. *Cellulose* **2020**, *27*, 5729−5743.
(19) Winter, H. H.; Chambon, F. Analysis of Linear Viscoelasticity of a Crosslinking Polymer at the Gel Point. *J. Rheol.* **1986**, *30*, 367−382.
(20) Chambon, F.; Winter, H. H. Linear viscoelasticity at the gel point of a crosslinking PDMS with imbalanced stoichiometry. *J. Rheol.* **1987**, *31*, 683−697.
(21) Martin, J. E.; Adolf, D.; Wilcoxon, J. P. Viscoelasticity of near-critical gels. *Phys. Rev. Lett.* **1988**, *61*, 2620.
(22) Adolf, D.; Martin, J. E. Time-cure superposition during crosslinking. *Macromolecules* **1990**, *23*, 3700−3704.
(23) Mours, M.; Winter, H. Time-resolved rheometry. *Rheol. Acta* **1994**, *33*, 385−397.
(24) Winter, H. H.; Morganelli, P.; Chambon, F. Stoichiometry effects on rheology of model polyurethanes at the gel point. *Macromolecules* **1988**, *21*, 532−535.
(25) Winter, H.; Mours, M. Rheology of polymers near liquid-solid transitions. *Adv. Polym. Sci.* **1997**, *134*, 165−230.
(26) Lennon, K. R.; McKinley, G. H.; Swan, J. W. A data-driven method for automated data superposition with applications in soft matter science. *Data-Centric Eng.* **2023**, *4*, No. e13.
(27) Larsen, T. H.; Furst, E. M. Microrheology of the liquid-solid transition during gelation. *Phys. Rev. Lett.* **2008**, *100*, 146001.
(28) Larsen, T.; Schultz, K.; Furst, E. M. Hydrogel microrheology near the liquid-solid transition. *Korea Aust. Rheol. J.* **2008**, *20*, 165−173.
(29) Chen, D.; Chen, K.; Hough, L.; Islam, M.; Yodh, A. Rheology of carbon nanotube networks during gelation. *Macromolecules* **2010**, *43*, 2048−2053.
(30) Hong, W.; Xu, G.; Ou, X.; Sun, W.; Wang, T.; Tong, Z. Colloidal probe dynamics in gelatin solution during the sol−gel transition. *Soft Matter* **2018**, *14*, 3694−3703.
(31) Keshavarz, B.; Rodrigues, D. G.; Champenois, J.-B.; Frith, M. G.; Ilavsky, J.; Geri, M.; Divoux, T.; McKinley, G. H.; Poulesquen, A. Time-connectivity superposition and the gel/glass duality of weak colloidal gels. *Proc. Natl. Acad. Sci. U.S.A.* **2021**, *118*, No. e2022339118.
(32) Bantawa, M.; Keshavarz, B.; Geri, M.; Bouzid, M.; Divoux, T.; McKinley, G. H.; Del Gado, E. The hidden hierarchical nature of soft particulate gels. *Nat. Phys.* **2023**, *19*, 1178.
(33) Jaishankar, A.; McKinley, G. H. Power-law rheology in the bulk and at the interface: quasi-properties and fractional constitutive equations. *Phys. Eng. Sci.* **2013**, *469*, 20120284.
(34) Bonfanti, A.; Kaplan, J. L.; Charras, G.; Kabla, A. Fractional viscoelastic models for power-law materials. *Soft Matter* **2020**, *16*, 6002−6020.
(35) Zaccone, A.; Winter, H.; Siebenbürger, M.; Ballauff, M. Linking self-assembly, rheology, and gel transition in attractive colloids. *J. Rheol.* **2014**, *58*, 1219−1244.
(36) Winter, H. Evolution of rheology during chemical gelation. *Prog. Colloid Polym. Sci.* **1987**, *75*, 104−110.
(37) Suman, K.; Joshi, Y. M. On the universality of the scaling relations during sol-gel transition. *J. Rheol.* **2020**, *64*, 863−877.
(38) Geri, M.; Keshavarz, B.; Divoux, T.; Clasen, C.; Curtis, D. J.; McKinley, G. H. Time-Resolved Mechanical Spectroscopy of Soft Materials via Optimally Windowed Chirps. *Phys. Rev. X* **2018**, *8*, 041042.
(39) Bouzid, M.; Keshavarz, B.; Geri, M.; Divoux, T.; Del Gado, E.; McKinley, G. H. Computing the linear viscoelastic properties of soft gels using an optimally windowed chirp protocol. *J. Rheol.* **2018**, *62*, 1037−1050.
(40) Morlet-Decarnin, L.; Divoux, T.; Manneville, S. Slow dynamics and time−composition superposition in gels of cellulose nanocrystals. *J. Chem. Phys.* **2022**, *156*, 214901.
(41) Reerink, H.; Overbeek, J. T. G. The rate of coagulation as a measure of the stability of silver iodide sols. *Discuss. Faraday Soc.* **1954**, *18*, 74−84.
(42) van der Linden, M.; Conchúir, B. O.; Spigone, E.; Niranjan, A.; Zaccone, A.; Cicuta, P. Microscopic Origin of the Hofmeister Effect in Gelation Kinetics of Colloidal Silica. *J. Phys. Chem. Lett.* **2015**, *6*, 2881−2887.
(43) Muthukumar, M. Screening effect on viscoelasticity near the gel point. *Macromolecules* **1989**, *22*, 4656−4658.
(44) De Gennes, P.-G. On a relation between percolation theory and the elasticity of gels. *J. Phys., Lett.* **1976**, *37*, 1−2.
(45) Adam, M.; Delsanti, M.; Durand, D.; Hild, G.; Munch, J. Mechanical properties near gelation threshold, comparison with classical and 3d percolation theories. *Pure Appl. Chem.* **1981**, *53*, 1489−1494.
(46) Stauffer, D.; Coniglio, A.; Adam, M. *In Polymer Networks*; Dušek, K., Ed.; Springer Berlin Heidelberg: Berlin, Heidelberg, 1982; pp 103−158.
(47) Axelos, M.; Kolb, M. Crosslinked biopolymers: Experimental evidence for scalar percolation theory. *Phys. Rev. Lett.* **1990**, *64*, 1457.

https://doi.org/10.1021/acsmacrolett.3c00536
ACS Macro Lett. 2023, 12, 1733−1738

(48) Hodgson, D. F.; Amis, E. J. Dynamic viscoelastic characterization of sol-gel reactions. *Macromolecules* **1990**, *23*, 2512−2519.
(49) Rouwhorst, J.; Ness, C.; Stoyanov, S.; Zaccone, A.; Schall, P. Nonequilibrium continuous phase transition in colloidal gelation with short-range attraction. *Nat. Commun.* **2020**, *11*, 3558.
(50) He, S.; Pascucci, D. R.; Caggioni, M.; Lindberg, S.; Schultz, K. M. Rheological properties of phase transitions in polydisperse and monodisperse colloidal rod systems. *AIChE J.* **2021**, *67*, No. e17401.

https://doi.org/10.1021/acsmacrolett.3c00536
ACS Macro Lett. 2023, 12, 1733−1738